

Tuning linear and nonlinear characteristics of a resonator via nonlinear interaction with a secondary resonator

**Oriel Shoshani, Mark I. Dykman &
Steven W. Shaw**

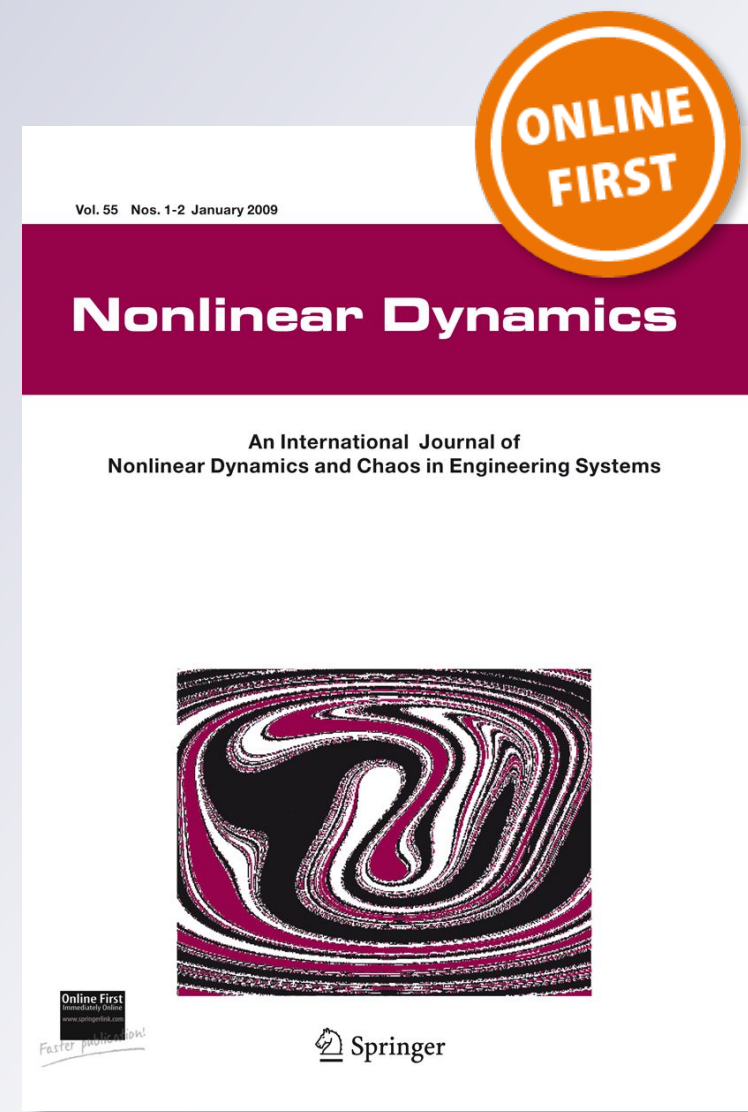
Nonlinear Dynamics

An International Journal of Nonlinear
Dynamics and Chaos in Engineering
Systems

ISSN 0924-090X

Nonlinear Dyn

DOI 10.1007/s11071-019-05194-0



 Springer

Your article is protected by copyright and all rights are held exclusively by Springer Nature B.V.. This e-offprint is for personal use only and shall not be self-archived in electronic repositories. If you wish to self-archive your article, please use the accepted manuscript version for posting on your own website. You may further deposit the accepted manuscript version in any repository, provided it is only made publicly available 12 months after official publication or later and provided acknowledgement is given to the original source of publication and a link is inserted to the published article on Springer's website. The link must be accompanied by the following text: "The final publication is available at link.springer.com".



Tuning linear and nonlinear characteristics of a resonator via nonlinear interaction with a secondary resonator

Oriel Shoshani · Mark I. Dykman · Steven W. Shaw

Received: 3 February 2019 / Accepted: 8 August 2019
© Springer Nature B.V. 2019

Abstract We consider the dynamics of a nonlinear resonator that is nonlinearly coupled to a linear resonator that has a relatively short decay time. In this case, the secondary (linear) resonator adiabatically tracks the primary (nonlinear) resonator. This model, which is motivated by ongoing experimental work in nano-resonators, is analyzed analytically and numerically to show that the linear and nonlinear characteristics of the primary resonator can be altered in a significant manner by the coupling to the secondary resonator. Such an arrangement may provide a practical means of tuning resonator characteristics in applications.

Keywords Nano- and micro-electromechanical systems · Nonlinear resonators · Tuning resonator characteristics

1 Introduction

Nano- and micro-electromechanical systems (N/MEMS) resonators are widely used in a variety of applications that include inertial sensing, signal processing, switching, and timing [1–4]. These devices possess inherent compatibility with semiconductor technology, the ability to fulfill miniaturization requirements, and offer some improved performance metrics when compared to their purely electrical analogs [5–8].

As the size of N/MEMS resonators is reduced, their vibrations become nonlinear already for small amplitudes [9]. Nonlinear stiffness effects in N/MEMS resonators commonly arise from multiple sources, such as finite deformations that lead to nonlinear strain–displacement relationships [10–12] and the nonlinear nature of the electrostatic forces in capacitive N/MEMS [13–15]. Nonlinear damping in N/MEMS resonators can be derived from a microscopic model, which account for nonlinear coupling between the resonator and a thermal bath [16, 17], or from a macroscopic model, which accounts for material viscoelasticity and geometric nonlinearities [18].

While the linear stiffness and linear damping, which are associated with the natural frequency and the nominal quality factor (or decay time), respectively, are of obvious interest for any resonant N/MEMS application, the nonlinear stiffness and nonlinear damping can also influence significantly the device figures of merits. Examples include the degradation of frequency

O. Shoshani (✉)
Ben-Gurion University of the Negev, 84105 Beer-Sheva, Israel
e-mail: oriel@bgu.ac.il

M. I. Dykman
Michigan State University, 567 Wilson Road, East Lansing, MI, USA
e-mail: dykman@pa.msu.edu

S. W. Shaw
Florida Institute of Technology, 150 W University Blvd, Melbourne, FL, USA
e-mail: sshaw@fit.edu

precision due to amplitude modulation (AM) to phase modulation (PM) conversion that arises from Duffing nonlinearity [19,20], and the degradation of nanotube and graphene nano-resonators quality factors due to nonlinear van der Pol-type damping [21].

Numerous studies considered different methods of tuning the linear and nonlinear characteristics of N/MEMS resonators. DeMartini et al. [22] experimentally demonstrated a means to tune linear and nonlinear characteristics of parametrically excited MEMS resonators by adjusting the drive DC and AC excitation voltages, and the configurations of their non-interdigitated capacitive comb fingers. Saghafi et al. [23] conducted a theoretical and numerical study of a bilayer microbeam and considered ways to tune the magnitude of intrinsic nonlinear effects and the beam dynamic range by varying the beam geometry. Li et al. [24] experimentally demonstrated a systematic control of the Duffing nonlinearity in MEMS resonators using shape optimization techniques.

Several experimental observations [25–27] have shown that when N/MEMS resonators are operated in 1:3 internal resonance conditions, the low-frequency vibrational mode can experience: (i) a significant frequency stabilization [25] (which implies that the effects of the Duffing nonlinearity are considerably reduced), (ii) an increase in the decay rate due to mode hybridization [26], and (iii) amplitude dwell in which the fast-frequency vibrational mode compensates for the low-frequency vibrational mode losses and practically eliminates its decay for a finite time [27]. In a recent study [28], the authors theoretically analyzed the 1:3 internal resonance of nanomechanical modes and showed that it can lead to a variety of anomalous decay behaviors, where both increase (as observed by [26]) and decrease (as observed by [27]) in the decay rate of the low-frequency mode can be obtained. Moreover, it was shown that the coupling between the two modes can result in an increase in the effective linear damping of the low-frequency mode for sufficiently large amplitude, even when the system is far from internal resonance [28]. In this work, we further theoretically explore such interactions and show that they can be used to tune the linear and nonlinear characteristics of a primary resonator when it is coupled to a relatively fast-decaying secondary resonator. The results developed here are related to the seminal work on a classical oscillators coupled to a bath of linear oscillators [29,30]. Furthermore, the results of the current anal-

ysis can be viewed as a special case, with important potential applications (e.g., manipulation of MEMS resonator characteristics), of the more general analyses of [16,31].

The paper is organized as follows: In Sect. 2, we formulate the problem and show that the motion of the relatively fast-decaying secondary resonator can be eliminated from the governing equation under the adiabatic approximation. In Sect. 3, we conduct an asymptotic analysis and obtain the main results of the paper, consisting of closed-form expressions for the modified linear and nonlinear characteristics of the primary resonator. In Sect. 4, we numerically validate our analytical predictions. In Sect. 5, we summarize our main findings and discuss their implications. We also include an appendix which briefly describes the microscopic theory of a resonator that interacts with a medium [16,19,32], since it provided the theoretical inspiration for the current work.

2 Problem formulation

We consider a system with two resonators that are mutually coupled. Figure 1 depicts a conceptual view of such a system with a simplified circuit schematic for the electronic realization of the coupling between the resonators. This realization, via electronic coupling, is chosen for the sake of clarity due to its simplicity; however, one can consider other types of coupling between the resonators, such as mechanical [33] and optical [34].

We assume that the primary resonator (with coordinate q_1) can experience a large amplitude oscillation around its stable equilibrium, $q_1 = 0$, and its potential $U(q_1)$, provides a nonlinear restoring force. The secondary resonator (with coordinate q_2) is linear and oscillates with small amplitude around its stable equilibrium, $q_2 = 0$. To be consistent with the above assumptions, we model the interaction potential of the two resonators as $U_{\text{inter}} = -q_2 G(q_1)$. Thus, the Hamiltonian of the system is given by

$$\mathcal{H} = p_1^2/2 + U(q_1) + p_2^2/2 + \omega_2^2 q_2^2/2 - q_2 G(q_1). \quad (1)$$

The equations of motion of the resonators with the inclusion of linear damping are formally given by \ddot{q}_k

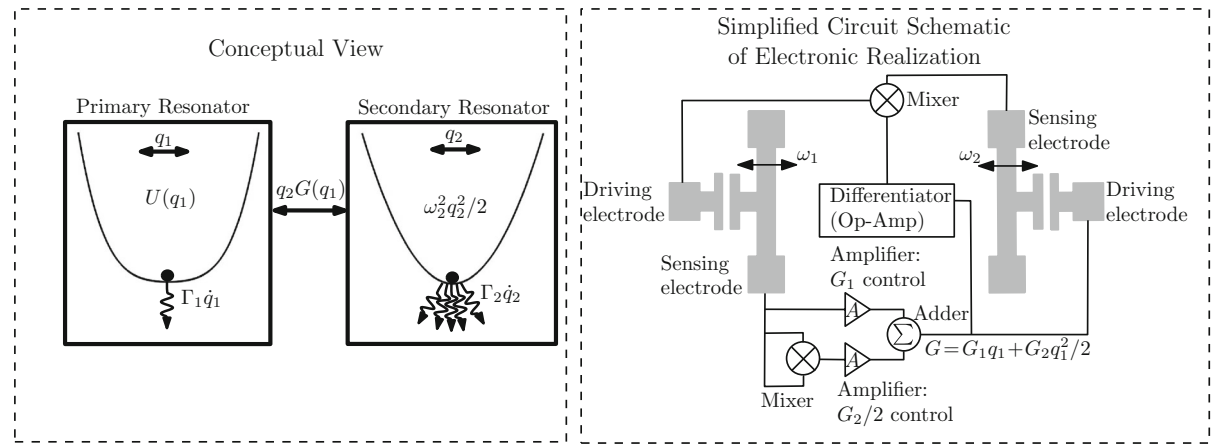


Fig. 1 Conceptual view and simplified circuit schematic of an electronic realization. Left panel: conceptually, the two resonators mutually and nonlinearly coupled via an interaction potential, $-q_2 G(q_1)$. The primary resonator (q_1) has a nonlinear conservative restoring force, $-U'(q_1)$, and weak linear dissipation, $-\Gamma_1 \dot{q}_1$. The bath resonator has a linear conservative restoring force, $-\omega_2^2 q_2$, and a relatively strong linear dissipation, $-\Gamma_2 \dot{q}_2$. Right panel: For micro-mechanical systems, the motion

of each resonator is detected using a parallel-plate capacitive sensing technique. The signal from the primary resonator is fed into a mixer, amplifiers (for control of different coefficients of G), and an adder to form the function $G(q_1)$. The signal $G(q_1)$ is then fed into the driving electrode of the bath resonator, and to a differentiator and a mixer, which multiplies the signal $G'(q_1)$ with q_2 , and finally, the mixed signal $q_2 G'(q_1)$ is being fed into the driving electrode of the primary resonator

$= \dot{p}_k = -2\Gamma_k \dot{q}_k - \partial \mathcal{H} / \partial q_k$ and can be explicitly written as

$$\ddot{q}_1 = -2\Gamma_1 \dot{q}_1 - U'(q_1) + q_2 G'(q_1), \quad (2)$$

$$\ddot{q}_2 = -2\Gamma_2 \dot{q}_2 - \omega_2^2 q_2 + G(q_1), \quad (3)$$

where the overdot denotes a time derivative, the prime symbol differentiation of a function with respect to its single variable, and $-2\Gamma_k \dot{q}_k$ models the linear friction force experienced by resonator k with $k = 1, 2$. Furthermore, we assume that both resonators are lightly damped ($\Gamma_k / \omega_k \ll 1$) and that the decay times satisfy $\Gamma_2 / \Gamma_1 \gg 1$ so that the secondary resonator will adiabatically track the primary resonator [28].

We formally solve Eq. (3) in terms of its Green's function, i.e.,

$$q_2(t) = e^{-\Gamma_2 t} \left[q_2(0) \cos(\omega_{2d} t) + \frac{p_2(0)}{\omega_{2d}} \sin(\omega_{2d} t) \right] + \frac{1}{\omega_{2d}} \int_0^t G(q_1(\tau)) e^{-\Gamma_2(t-\tau)} \sin(\omega_{2d}(t-\tau)) d\tau, \quad (4)$$

where, due to the low level of damping in the system ($\Gamma_k / \omega_k \ll 1$), we approximate the secondary resonator

damped eigenfrequency ω_{2d} by its undamped eigenfrequency ω_2 , i.e., $\omega_{2d} = \omega_2 \sqrt{1 - (\Gamma_2 / \omega_2)^2} \approx \omega_2$. Upon inserting Eq. (4) into Eq. (2), we find that

$$\ddot{q}_1 = -2\Gamma_1 \dot{q}_1 - U'(q_1) + G'(q_1)(L[q_1] + F), \quad (5)$$

where

$$L[q_1] = \frac{1}{\omega_2} \int_0^t G(q_1(\tau)) e^{-\Gamma_2(t-\tau)} \sin(\omega_2(t-\tau)) d\tau, \quad (6)$$

$$F(t) = e^{-\Gamma_2 t} \left[q_2(0) \cos(\omega_2 t) + \frac{p_2(0)}{\omega_2} \sin(\omega_2 t) \right]. \quad (7)$$

The functional $L[q_1]$ describes the retarded reaction of the secondary resonator on the primary resonator, and $F(t)$ describes the response of the primary resonator to the initial state of the secondary resonator.

3 Asymptotic analysis

For weakly nonlinear interaction between the resonators, we can use the method of averaging [35, 36], i.e., we assume that $q_1(t) = \mathcal{A}(t) e^{i\omega_1 t} + \mathcal{A}^*(t) e^{-i\omega_1 t}$

and $\dot{q}_1(t) = i\omega_1[\mathcal{A}(t)e^{i\omega_1 t} - \mathcal{A}^*(t)e^{-i\omega_1 t}]$, where \mathcal{A}^* is the complex conjugate of \mathcal{A} , and the complex amplitude $\mathcal{A}(t)$ remains almost constant over the period $T = 2\pi/\omega_1$ of the linearized resonator, $\omega_1^2 = U''(0)$. Thus, $G(q_1(t))$ can be replaced by its Fourier series $G(q_1(t)) = \sum_n c_n(\mathcal{A}(t), \mathcal{A}^*(t))e^{in\omega_1 t}$, where $c_{-n} = c_n^*$. Consequently, the functional $L[q_1]$ can be rewritten as

$$L[q_1] = \int_0^t \sum_n \frac{c_n(\tau)}{2i\omega_2} [e^{-\Gamma_2(t-\tau)+i[n\omega_1\tau+\omega_2(t-\tau)]} - e^{-\Gamma_2(t-\tau)+i[n\omega_1\tau-\omega_2(t-\tau)]}] d\tau. \quad (8)$$

Since $c_n(t)$ are functions of $\mathcal{A}(t)$ and $\mathcal{A}^*(t)$, they also vary slowly in time. Thus, to the leading order we can approximate Eq. (8) as follows:

$$\begin{aligned} L[q_1] &\approx \sum_n \frac{c_n(t)}{2i\omega_2} \int_0^t [e^{-\Gamma_2(t-\tau)+i[n\omega_1\tau+\omega_2(t-\tau)]} - e^{-\Gamma_2(t-\tau)+i[n\omega_1\tau-\omega_2(t-\tau)]}] d\tau \\ &= \sum_n \frac{c_n(t)}{2\omega_2} e^{in\omega_1 t} \left[\frac{1 - e^{-[\Gamma_2+i(n\omega_1-\omega_2)]t}}{-(n\omega_1 - \omega_2) + i\Gamma_2} + \frac{1 - e^{-[\Gamma_2+i(n\omega_1+\omega_2)]t}}{(n\omega_1 + \omega_2) - i\Gamma_2} \right]. \end{aligned} \quad (9)$$

For times that are larger than the relaxation time of the secondary resonator, $t \gg \Gamma_2^{-1}$, the functional $L[q_1]$ is further simplified and yields

$$L[q_1] \approx \sum_n \frac{\omega_2^2 - n^2\omega_1^2 - 2in\omega_1\Gamma_2}{(\omega_2^2 - n^2\omega_1^2)^2 + (2n\omega_1\Gamma_2)^2} c_n(t) e^{in\omega_1 t}. \quad (10)$$

Hence, for $t \gg \Gamma_2^{-1}$, the equation of motion of the primary resonator, Eq. (5), reduces to

$$\begin{aligned} \ddot{q}_1 + U'(q_1) &= -2\Gamma_1\dot{q}_1 + G'(q_1) \\ &\quad \sum_n \frac{\omega_2^2 - n^2\omega_1^2 - 2in\omega_1\Gamma_2}{(\omega_2^2 - n^2\omega_1^2)^2 + (2n\omega_1\Gamma_2)^2} c_n(t) e^{in\omega_1 t}. \end{aligned} \quad (11)$$

This approximation applies even for resonant situations, where ω_2 is close to a multiple of ω_1 .

In what follows, we focus only on times that are larger than the relaxation time of the secondary resonator, $t \gg \Gamma_2^{-1}$, where the secondary resonator is adiabatically tracking the primary resonator and acts as a thermal reservoir. In fact, we have also assumed

here that the functions $c_n(t)$ vary slowly over the time Γ_2^{-1} . This is a restriction on the nonlinearity and the decay rate of the primary resonator.

For the weak coupling that we consider, the only terms to keep in the sum over n in Eq. (11) are the resonant terms, which oscillate, with the slowly varying amplitude and phase, at the same frequency as $q_1(t)$. For $G' = \text{constant}$, these are terms with $n = \pm 1$,

whereas if we take into account the term $\propto q_1$ in $G'(q_1)$, we have to keep the resonant terms with $n = \pm 2$ and $n = 0$. This is used in the calculation in the next section.

3.1 Essential leading-order nonlinear terms

Restricting our attention to the essential leading-order nonlinear terms, we take $U(q_1) = \omega_1^2 q_1^2/2 + \gamma q_1^4/4$; the non-secular term $\beta q_1^3/3$ renormalizes γ , to the second order in β , which we assume to have been taken into account. Furthermore, we assume that $G(q_1)$ can be similarly represented, $G(q_1) = G_1 q_1 + G_2 q_1^2/2 + O(q_1^3)$, where $G_1 \equiv G'(0)$ and $G_2 \equiv G''(0)$. Consequently, we obtain the following approximated equation for the complex amplitude of the primary resonator

$$\begin{aligned} \dot{\mathcal{A}} &= -\Gamma_1 \mathcal{A} \left(1 + \alpha_1 \frac{\Gamma_2}{\Gamma_1} + \alpha_2 \frac{\Gamma_2}{\Gamma_1} |\mathcal{A}|^2 \right) \\ &\quad - i \mathcal{A} \left\{ \alpha_1 \left(\frac{\omega_2^2 - \omega_1^2}{2\omega_1} \right) + \left[\alpha_2 \left(\frac{3\omega_2^2 - 20\omega_1^2}{4\omega_1} \right. \right. \right. \\ &\quad \left. \left. \left. + \frac{8\omega_1}{\omega_2^2} (\Gamma_2^2 + \omega_1^2) \right) - \frac{3\gamma}{2\omega_1} \right] |\mathcal{A}|^2 \right\}, \end{aligned} \quad (12)$$

where the coupling to the secondary resonator is captured by the terms with coefficients

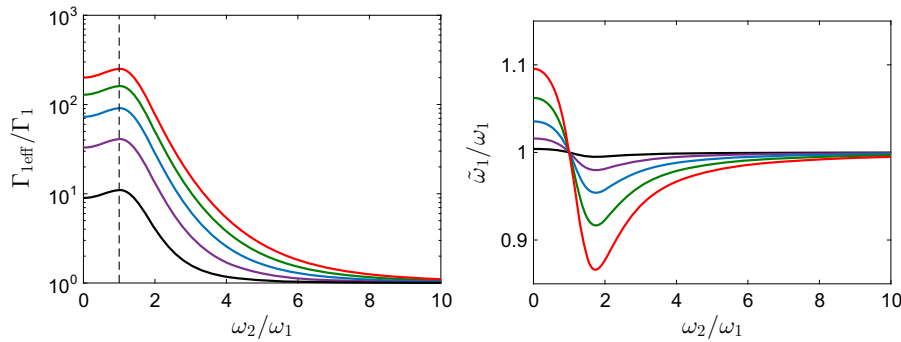


Fig. 2 Variation in the normalized linear damping ($\Gamma_{1\text{eff}}/\Gamma_1$) and frequency ($\tilde{\omega}_1/\omega_1$) parameters of the primary resonator as a function of the normalized eigenfrequency of the secondary resonator (ω_2/ω_1) for $\Gamma_2/\Gamma_1 = 10^3$ and different levels of the linear coupling strength: $G_1 = 0.2$ (black), $G_1 = 0.4$ (purple), $G_1 = 0.6$ (blue), $G_1 = 0.8$ (green), and $G_1 = 1$ (red). Left panel: The effective linear damping reaches its maximum value when the

two resonators interact resonantly at $\omega_2/\omega_1 = 1$ (indicated by the vertical dashed line). Right panel: The primary resonator shifted eigenfrequency increases for $\omega_2 < \omega_1$ and decreases for $\omega_2 > \omega_1$. We emphasize that the theory applies for weak coupling of the resonators, which means that we only study the regime where $|\tilde{\omega}_1 - \omega_1| \ll \omega_1$. (Color figure online)

$$\begin{aligned} \alpha_1 &= \frac{G_1^2}{(\omega_2^2 - \omega_1^2)^2 + (2\Gamma_2\omega_1)^2}, \\ \alpha_2 &= \frac{G_2^2}{(\omega_2^2 - 4\omega_1^2)^2 + (4\Gamma_2\omega_1)^2}. \end{aligned} \quad (13)$$

From Eq. (12), we deduce that the interaction of the primary resonator with the secondary resonator modifies the linear and nonlinear terms in the equation of motion for the coordinate q_1 of the primary resonator. To be specific, we see that at the leading order, the interaction between the two resonators leads to the following changes in this equation: (i) an increase in the linear decay rate $\Gamma_{1\text{eff}} = \Gamma_1 + \alpha_1\Gamma_2$; (ii) the addition of new nonlinear cubic (van der Pol type) damping term $-\alpha_2\Gamma_2|\mathcal{A}|^2\mathcal{A}$; (iii) a shift in the eigenfrequency $\Delta\omega_1 = \alpha_1(\omega_2^2 - \omega_1^2)/(2\omega_1)$; and (iv) a modification to the Duffing nonlinearity $-i\alpha_2[(3\omega_2^2 - 20\omega_1^2)/(4\omega_1) + 8\omega_1(\Gamma_2^2 + \omega_1^2)/\omega_2^2]|\mathcal{A}|^2\mathcal{A}$. Hence, Eq. (12) is consistent with the complex amplitude equation that one gets from the averaging method for the following phenomenological model

$$\ddot{q}_1 + 2(\Gamma_{1\text{eff}}\dot{q}_1 + \alpha_2\Gamma_2q_1^2)\dot{q}_1 + \tilde{\omega}_1^2q_1 + \tilde{\gamma}q_1^3 = 0, \quad (14)$$

where the square of the shifted eigenfrequency is given by $\tilde{\omega}_1^2 = \omega_1^2 - \alpha_1(\omega_2^2 - \omega_1^2)$, and the modified Duffing parameter is given by $\tilde{\gamma} = \gamma - \frac{2}{3}\alpha_2[(3\omega_2^2 - 20\omega_1^2)/4 + 8\omega_1^2(\Gamma_2^2 + \omega_1^2)/\omega_2^2]$.

We note that the linear characteristics (i.e., the linear damping and eigenfrequency) are functions of the linear coupling strength G_1 and therefore can be tuned by variation of G_1 (Fig. 2). Due to the presence of a Lorentzian function $\alpha_1(\omega_2)$ in the effective linear damping $\Gamma_{1\text{eff}} = \Gamma_1 + \alpha_1\Gamma_2$, it reaches a maximum value when the eigenfrequencies of the isolated secondary and primary resonators are equal, $\omega_2 = \omega_1$. This result is not surprising as it corresponds to a resonant interaction between the resonators, which only occurs when $\omega_2 \approx \omega_1$ for linear coupling. Alternatively, this coupling-induced decay rate can be understood in terms of the standard Fermi golden rule [37]. It is quadratic in the linear coupling strength G_1 and is proportional to the “density of states” $1/[(\omega_2^2 - \omega_1^2)^2 + (2\Gamma_2\omega_1)^2]$ of the effective reservoir provided by the secondary resonator. The primary resonator shifted eigenfrequency $\tilde{\omega}_1$ increases for $\omega_2 < \omega_1$ and decreases for $\omega_2 > \omega_1$. This change in the shifted eigenfrequency $\tilde{\omega}_1$ can be related to a linear anti-crossing (eigenvalue veering) with a frequency splitting of the two eigenfrequencies of the linearly coupled ($G_1 \neq 0$, $G_2 = 0$) dynamical system [38].

Similarly, the nonlinear characteristics (i.e., the van der Pol damping and modified Duffing parameter) are functions of the nonlinear quadratic coupling strength G_2 and therefore can be tuned by variation of G_2 (Fig. 3). Due to the presence of a Lorentzian function $\alpha_2(\omega_2)$ in the van der Pol damping term $2\alpha_2\Gamma_2q_1^2\dot{q}_1$, it reaches a maximum value when the eigenfrequency of

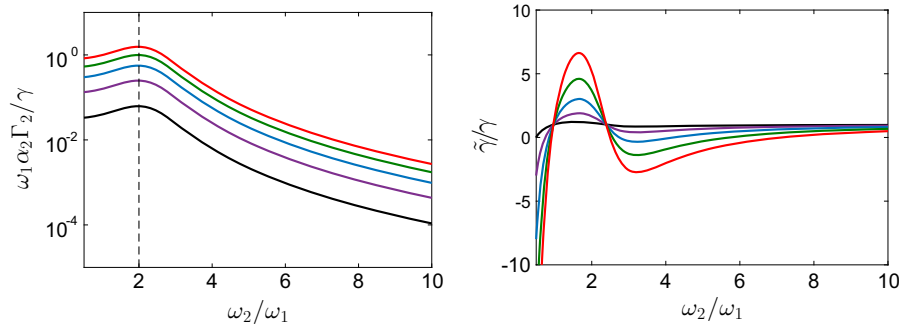


Fig. 3 Variation in the normalized nonlinear damping ($\omega_1 \alpha_2 \Gamma_2 / \gamma$) and stiffness (i.e., Duffing, $\tilde{\gamma} / \gamma$) parameters of the primary resonator as a function of the normalized eigenfrequency of the secondary resonator (ω_2 / ω_1) for $\Gamma_2 / \Gamma_1 = 10^3$, $\gamma = 1$ and different levels of the nonlinear coupling strength: $G_2 = 1$ (black), $G_2 = 2$ (purple), $G_2 = 3$ (blue), $G_2 = 4$ (green), and

$G_2 = 5$ (red). Left panels: The van der Pol damping reaches its maximum value when the two resonators interact resonantly at $\omega_2 / \omega_1 = 2$ (indicated by the vertical dashed line). Right panel: The modified Duffing parameter $\tilde{\gamma}$ can deviate dramatically from its nominal value γ at relatively low frequencies of the secondary resonator and can even change sign. (Color figure online)

the secondary resonator is close to twice the eigenfrequency of the primary resonator, $\omega_2 \approx 2\omega_1$. The result can be understood as a nonlinear resonant interaction between the resonators, which can only occur when $\omega_2 \approx 2\omega_1$ for this type of quadratic coupling, provided $\Gamma_1 \ll \omega_1$ and $\Gamma_2 \ll \omega_2$. Alternatively, this can also be understood in terms of the Fermi golden rule, where G_2 is the “matrix element” of the interaction and $1/[(\omega_2^2 - 4\omega_1^2)^2 + (4\Gamma_2\omega_1)^2]$ is the “density of states” of the effective reservoir provided by the secondary resonator at twice the eigenfrequency of the primary resonator. The modified Duffing parameter $\tilde{\gamma}$ can deviate dramatically from its nominal value γ for a range of frequency ratios of the resonators ($\omega_2 / \omega_1 < 5$) and in the vicinity of the nonlinear resonance condition ($\omega_2 = 2\omega_1$). More importantly, it can also change sign, i.e., changing from hardening nonlinearity ($\tilde{\gamma} > 0$) to softening nonlinearity ($\tilde{\gamma} < 0$). This variation of $\tilde{\gamma}$ leads to a peculiar change in the effective vibration frequency $\omega_1^{\text{eff}} \approx \tilde{\omega}_1 + 3\tilde{\gamma}|\mathcal{A}|^2/2\tilde{\omega}_1$, which is attributed to a nonlinear counterpart of frequency anti-crossing due to nonlinear resonance [28]. However, as we show in the following subsection, even for significantly higher frequencies (say, $\omega_2 / \omega_1 = 10$), which are far from nonlinear resonance conditions, $\tilde{\gamma}$ can be twofold smaller than its nominal value γ .

3.2 Analytical solution of the complex amplitude equation

Equation (12) yields the following pair of evolution equations for the complex amplitude modulus and argument ($\mathcal{A} = |\mathcal{A}|e^{i\phi}$)

$$|\dot{\mathcal{A}}| = -|\mathcal{A}|(\Gamma_{\text{eff}} + \alpha_2 \Gamma_2 |\mathcal{A}|^2), \quad (15)$$

$$\dot{\phi} = -\Delta\omega_1 + \frac{3\tilde{\gamma}}{2\omega_1} |\mathcal{A}|^2. \quad (16)$$

Equations (15)–(16) can be solved in closed form

$$|\mathcal{A}(t)| = |\mathcal{A}(0)|e^{-\Gamma_{\text{eff}}t} \left[1 + \frac{\alpha_2 \Gamma_2}{\Gamma_{\text{eff}}} |\mathcal{A}(0)|^2 (1 - e^{-2\Gamma_{\text{eff}}t}) \right]^{-1/2}, \quad (17)$$

$$\phi(t) = \phi(0) - \Delta\omega_1 t + \frac{3\tilde{\gamma}}{4\omega_1 \alpha_2 \Gamma_2} \ln \left[1 + \frac{\alpha_2 \Gamma_2}{\Gamma_{\text{eff}}} |\mathcal{A}(0)|^2 (1 - e^{-2\Gamma_{\text{eff}}t}) \right]. \quad (18)$$

From the closed-form solution of the amplitude (modulus), Eq. (17), we can deduce the following: due to the presence of the van der Pol damping ($-\alpha_2\Gamma_2|\mathcal{A}|^2\mathcal{A}$), which arises from the nonlinear interaction (G_2, α_2) between q_1 and q_2 , we see that if $\alpha_2\Gamma_2|\mathcal{A}(0)|^2/\Gamma_{\text{eff}} \sim O(1)$ or bigger, then the amplitude of the primary resonator ($2|\mathcal{A}(t)|$) will decay in a non-exponential manner (faster than exponential), and the decay will become exponential only for large time, where $t \gg \Gamma_{\text{eff}}^{-1}$. These asymptotic non-exponential and exponential decays of the amplitude are given by

$$|\mathcal{A}(t)| = |\mathcal{A}(0)| [1 + 2\alpha_2\Gamma_2|\mathcal{A}(0)|^2t]^{-1/2} \quad \text{for } \Gamma_{\text{eff}}t \ll 1, \quad (19)$$

$$|\mathcal{A}(t)| = \sqrt{\frac{\Gamma_{\text{eff}}|\mathcal{A}(0)|^2}{\Gamma_{\text{eff}} + \alpha_2\Gamma_2|\mathcal{A}(0)|^2}} e^{-\Gamma_{\text{eff}}t} \quad \text{for } \Gamma_{\text{eff}}t \gg 1. \quad (20)$$

Similarly, from the closed-form solution of the phase (argument), Eq. (18), we deduce the following: For $\tilde{\gamma}/\gamma \neq 1$ and $3(\tilde{\gamma} - \gamma)/(4\omega_1\alpha_2\Gamma_2) \sim O(1)$ or bigger, the phase dynamics is highly affected by the nonlinear interaction (G_2, α_2) between q_1 and q_2 , and for large time, where $t \gg \Gamma_{\text{eff}}^{-1}$, there is only a linear shift of the eigenfrequency due to the linear interaction of the resonators (G_1, α_1). These asymptotic behaviors of the phase are given by

$$\phi(t) = \phi(0) + \frac{3\tilde{\gamma}}{4\omega_1\alpha_2\Gamma_2} \ln \left[1 + \frac{\alpha_2\Gamma_2}{\Gamma_{\text{eff}}} |\mathcal{A}(0)|^2 (1 - e^{-2\Gamma_{\text{eff}}t}) \right] \quad \text{for } \Gamma_{\text{eff}}t \ll 1, \quad (21)$$

$$\phi(t) = \phi(0) + \frac{3\tilde{\gamma}}{4\omega_1\alpha_2\Gamma_2} \ln \left[1 + \frac{\alpha_2\Gamma_2}{\Gamma_{\text{eff}}} |\mathcal{A}(0)|^2 \right] - \Delta\omega_1 t \quad \text{for } \Gamma_{\text{eff}}t \gg 1 \quad (22)$$

In the remainder of this paper, we use a fixed set of system parameters: $\omega_1 = 1$, $\omega_2 = 10$, $\Gamma_1 = 10^{-3}$, $\Gamma_2 = 1$, $G_1 = 4$, $G_2 = 5$, $\gamma = 1$, to illustrate the linear and nonlinear characteristics of the primary resonator. Figure 4 depicts the amplitude and phase dynamics of the primary resonator for the initial conditions $\mathcal{A}(0) = 10i$. Due to the linear interaction of the resonators (G_1, α_1), there is almost a three-fold increase in the linear decay rate $\Gamma_{\text{eff}}/\Gamma_1 = 2.63$,

and the eigenfrequency is shifted downward by 8%, $\Delta\omega_1/\omega_1 = 0.08$. The nonlinear interaction of the resonators (G_2, α_2) is responsible for the van der Pol nonlinear damping term with a coefficient of $\alpha_2\Gamma_2 = 2.7 \times 10^{-3}$, which significantly changes the amplitude dynamics and leads to a non-exponential decay, and for a twofold decrease in the Duffing parameter $\tilde{\gamma}/\gamma = 0.49$. The asymptotic behaviors of Eqs. (19)–(22) clearly govern the amplitude and phase dynamics at small and large times.

4 Numerical validation

To validate our single-mode theoretical approximation, we rewrite the full equations, Eqs. (2)–(3), in terms of the complex amplitudes, i.e., $q_k(t) = A_k(t)e^{i\omega_k t} + A_k^*(t)e^{-i\omega_k t}$ and $\dot{q}_k(t) = i\omega_k[A_k(t)e^{i\omega_k t} - A_k^*(t)e^{-i\omega_k t}]$, where $k = 1, 2$, and set $U(q_1) = \omega_1^2 q_1^2/2 + \gamma q_1^4/4$, $G(q_1) = G_1 q_1 + G_2 q_1^2/2$. Thus, we obtain the following equations for the evolution of the complex amplitudes

$$\dot{A}_1 = \frac{e^{-i\omega_1 t}}{2i\omega_1} [q_2(G_1 + G_2 q_1) - \gamma q_1^3 - 2\Gamma_1 \dot{q}_1], \quad (23)$$

$$\dot{A}_2 = \frac{e^{-i\omega_2 t}}{2i\omega_2} \left[\left(G_1 + \frac{G_2}{2} q_1 \right) q_1 - 2\Gamma_2 \dot{q}_2 \right]. \quad (24)$$

Note that no approximations were made in the derivation of Eqs. (23)–(24), and they yield exact solutions for the complex amplitudes, $A_1(t)$ and $A_2(t)$, of the full equations, Eqs. (2)–(3). Hence, by solving Eqs. (23)–(24) numerically we can confirm the approximate asymptotic behavior of the complex amplitude, $\mathcal{A}(t) = |\mathcal{A}(t)|e^{i\phi(t)}$, given by Eqs. (17)–(18). Figure 5 shows a comparison between the numerically calculated exact equations and the theoretical approximation for the same system parameters as in Fig. 4 ($\omega_1 = 1$, $\omega_2 = 10$, $\Gamma_1 = 10^{-3}$, $\Gamma_2 = 1$, $G_1 = 4$, $G_2 = 5$, $\gamma = 1$) and three different initial conditions: (i) High initial energy of the primary resonator— $A_1(0) = 10i$ and $A_2(0) = 0.01$. (ii) Moderate initial energy of the primary resonator— $A_1(0) = i$ and $A_2(0) = 0.01$, and (iii) low initial energy of the primary resonator— $A_1(0) = 0.1i$, $A_2(0) = 0.01$. Note that these three cases can actually be captured by a single case starting from high initial energy of the primary resonator; however, for the sake of exposition, we treat them separately.

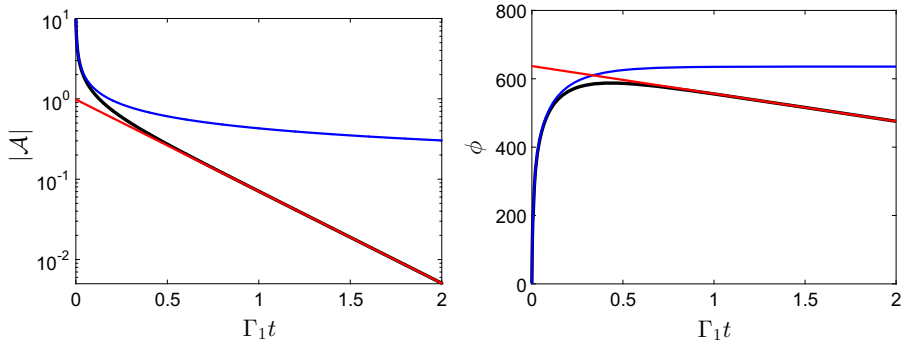


Fig. 4 Analytical estimations of the amplitude and phase dynamics of the primary resonator. Left panel: amplitude dynamics according to the closed-form solution (black curve) Eq. (17) and its asymptotic behaviors for $t \rightarrow 0$ (blue curve), i.e., $\phi(0) + \frac{3\tilde{\gamma}}{4\omega_1\alpha_2\Gamma_2} \ln \left[1 + \frac{\alpha_2\Gamma_2}{\Gamma_{\text{leff}}} |\mathcal{A}(0)|^2 (1 - e^{-2\Gamma_{\text{leff}}t}) \right]$, and $t \rightarrow \infty$ (red curve), i.e., $|\mathcal{A}(0)| \left[1 + 2\alpha_2\Gamma_2 |\mathcal{A}(0)|^2 t \right]^{-1/2}$, and $t \rightarrow \infty$ (red curve), i.e., $\sqrt{\frac{\Gamma_{\text{leff}} |\mathcal{A}(0)|^2}{\Gamma_{\text{leff}} + \alpha_2\Gamma_2 |\mathcal{A}(0)|^2}} e^{-\Gamma_{\text{leff}}t}$. Right panel: Phase dynamics accord-

ing to the closed-form solution (black curve) Eq. (18) and its asymptotic behaviors for $t \rightarrow 0$ (blue curve), i.e., $\phi(0) + \frac{3\tilde{\gamma}}{4\omega_1\alpha_2\Gamma_2} \ln \left[1 + \frac{\alpha_2\Gamma_2}{\Gamma_{\text{leff}}} |\mathcal{A}(0)|^2 (1 - e^{-2\Gamma_{\text{leff}}t}) \right]$, and $t \rightarrow \infty$ (red curve), i.e., $\phi(0) + \frac{3\tilde{\gamma}}{4\omega_1\alpha_2\Gamma_2} \ln \left[1 + \frac{\alpha_2\Gamma_2}{\Gamma_{\text{leff}}} |\mathcal{A}(0)|^2 \right] - \Delta\omega_1 t$. (Color figure online)

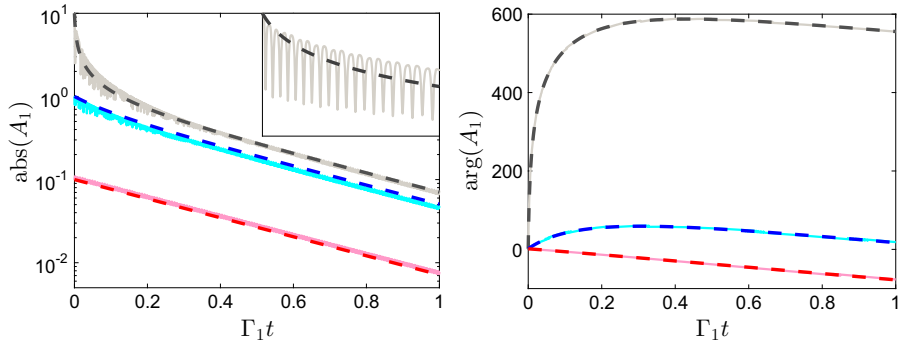


Fig. 5 Numerical and theoretical predictions of the amplitude and phase dynamics of the primary resonator. The amplitude (left panel) and phase (right panel) dynamics are shown for three different initial conditions: (i) $A_1(0) = 10i$, $A_2(0) = 0.01$ —gray curves, (ii) $A_1(0) = i$, $A_2(0) = 0.01$ —blue curves, and (iii) $A_1(0) = 0.1i$, $A_2(0) = 0.01$ —red curves. The light solid

curves indicate the result of the direct numerical integration of Eqs. (23)–(24), and the dark dashed curves indicate the theoretical predictions from Eqs. (17)–(18). The inset in the left panel shows the time evolution of the amplitude on the time interval $0 < \Gamma_1 t < 0.02$

Direct numerical integration of the full equations and the theoretical estimates are in excellent agreement (Fig. 5). In fact, the only clear difference between the numerics and the theory is the presence of fast oscillations that appear in the numerical solutions of the amplitude and phase (see the inset of the left panel in Fig. 5) due to the presence of non-secular terms that are not filtered out in the full equations, Eqs. (23)–(24). The numerical results also confirm that the nonlinear effects are most pronounced for high initial energy of the pri-

mary resonator ($|A_1(0)|^2$), that is, at the beginning of the ring down ($t \rightarrow 0$), and as the system decays toward its zero energy state ($t \rightarrow \infty$), only linear effects persist. Note that the current numerical integration only validates the theory for a specific set of parameters and hence can be considered only as a validation to the proof of concept. A detailed numerical analysis that includes parameter sensitivity analysis and numerical investigation of the theory limitations are out of the scope of the current paper and will be considered in future studies.

5 Closing remarks

In this paper, we analyzed the nonlinear interaction of mutually coupled resonators with significantly different decay rates, namely slowly decaying nonlinear (primary) resonator, which is nonlinearly coupled to a relatively fast-decaying linear resonator. We showed that such an interaction can change both the linear and nonlinear characteristics of the primary resonator. That is, by coupling a nonlinear resonator to relatively fast-decaying linear resonator, we can change its eigenfrequency, linear damping, and Duffing parameter and add new nonlinear van der Pol damping term to the resonator dynamics.

Theoretically, we view this interaction between resonators with significantly different decay rates as a discrete and finite version of the microscopic theory of a resonator that interacts with a medium, where the “medium” is the secondary resonator. Due to the nature of this interaction (only two resonators), the modified linear and nonlinear characteristics of the primary resonator depend on the eigenfrequency of the secondary resonator rather than on a continuous spectrum as in the standard case, in which the medium is modeled by infinite number of harmonic oscillators (see “Appendix” for brief description of the standard model of the bath with a large number of degrees of freedom and with a quasi-continuous frequency spectrum).

Practically, the results of this paper show a potential method for tuning parameters in nano- and micro-mechanical systems, allowing one to adjust the response of a resonator according to desired specifications by controlling its interaction with a fast-decaying linear resonator. This ability to tailor a desired nonlinear response of a resonator can be extremely useful in NEMS and MEMS applications. A prime example is in the case of closed loop oscillators used in timekeeping, and the ability to reduce the Duffing nonlinearity is an important step in reducing noise [39–42].

Funding SWS acknowledges partial support from the National Science Foundation (Grants Nos. CMMI 1561829 and CMMI 1662619). MID acknowledges partial support from the National Science Foundation (Grants Nos. CMMI 1661618 and DMR 1806473).

Compliance with ethical standards

Conflict of interest The authors declare that they have no conflict of interest.

Appendix A: Brief description of the microscopic theory of a resonator that interacts with a medium

We consider the total Hamiltonian of a nonlinear resonator with a potential $U(x)$ that is coupled to a medium of harmonic oscillators. The analysis is well-known [16, 19, 31, 32, 43–46]; here, we briefly outline it for completeness. The total Hamiltonian includes the resonator Hamiltonian \mathcal{H}_r , the medium Hamiltonian \mathcal{H}_m , and the interaction Hamiltonian $\mathcal{H}_{\text{inter}}$ and reads

$$\mathcal{H} = \frac{v^2}{2} + U(x) + \frac{1}{2} \sum_k (p_k^2 + \omega_k^2 q_k^2) - G(x) \sum_k \epsilon_k q_k. \quad (25)$$

The equations of motion resulting from Eq. (25) are

$$\ddot{x} = -U'(x) + G'(x) \sum_k \epsilon_k q_k, \quad (26)$$

$$\ddot{q}_k = -\omega_k^2 q_k + \epsilon_k G(x). \quad (27)$$

We formally solve Eq. (27) in terms of its Green's function, i.e.,

$$q_k(t) = q_k(0) \cos(\omega_k t) + \frac{p_k(0)}{\omega_k} \sin(\omega_k t) + \frac{\epsilon_k}{\omega_k} \int_0^t G(x(\tau)) \sin(\omega_k(t - \tau)) d\tau. \quad (28)$$

Upon inserting Eq. (28) into Eq. (26), we find that

$$\ddot{x} = -U'(x) + G'(x)(L[x] + F), \quad (29)$$

where

$$L[x] = \sum_k \frac{\epsilon_k^2}{\omega_k} \int_0^t G(x(\tau)) \sin(\omega_k(t - \tau)) d\tau, \quad (30)$$

$$F(t) = \sum_k \epsilon_k \left[q_k(0) \cos(\omega_k t) + \frac{p_k(0)}{\omega_k} \sin(\omega_k t) \right]. \quad (31)$$

Using integration by parts, we can rewrite Eq. (30) as

$$L[x] = -G(x(t)) \sum_k \frac{\epsilon_k^2}{\omega_k^2} + G(x(0)) \sum_k \frac{\epsilon_k^2}{\omega_k^2} \cos(\omega_k t) - \sum_k \frac{\epsilon_k^2}{\omega_k^2} \int_0^t \dot{x}(\tau) G'(x(\tau)) \cos(\omega_k(t-\tau)) d\tau. \quad (32)$$

We assume that the medium contains an infinite number of harmonic oscillators with a continuous spectrum. Consequently, we approximate the sum over k as an integral. Toward this end, we define the spectral density of the bath as $g(\omega) d\omega = \sum_{\omega < \omega_k < \omega + d\omega} \epsilon_k^2 / \omega_k^2$.

Using Eq. (32) along with the assumption of a continuous spectrum of the medium, we rewrite Eq. (29) as

$$\ddot{x} + G'(x) \int_0^t \Gamma(t-\tau) \dot{x}(\tau) G'(x(\tau)) d\tau + V'_{\text{ren}}(x) = G'(x) \tilde{F}, \quad (33)$$

where $\Gamma(t-\tau) = \int_{-\infty}^{\infty} g(\omega) \cos(\omega(t-\tau)) d\omega$ is the memory of the friction, $V_{\text{ren}}(x) = U(x) + \frac{1}{2} G^2(x) \int_{-\infty}^{\infty} g(\omega) d\omega$ is the renormalized potential of the resonator, and $\tilde{F} = F + G(x(0)) \int_{-\infty}^{\infty} g(\omega) \cos(\omega t) d\omega$ is a noise term.

The statistical properties of the noise term F are determined as follows: We assume that at $t = 0$, the interaction between the bath and the resonator is turned on and considers an ensemble of initial states in which $x(0)$ is held fixed but the initial bath variables $q_k(0)$, $p_k(0)$ are drawn at random from a canonical distribution characterized by a temperature T , i.e.,

$$\mathcal{P}(q_k, p_k | x(0) = x) \propto e^{-\mathcal{H}_m / k_B T}. \quad (34)$$

With this conditional probability for the bath variables, the noise term F obeys the fluctuation–dissipation relations

$$\langle F \rangle_{\mathcal{P}} = 0, \quad \langle F(t) F(\tau) \rangle_{\mathcal{P}} = k_B T \Gamma(t-\tau), \quad (35)$$

and hence, it is a colored Gaussian noise. Note that for a flat spectrum of the bath weighted with the coupling (the so-called Ohmic dissipation), we can use the Markovian approximation, where $\Gamma(t-\tau) = 2\langle g \rangle \delta(t-\tau)$ and $\langle g \rangle / \pi$ is the averaged value of the spectrum. Hence, Eq. (33) reduces to

$$\ddot{x} + 2\langle g \rangle G'^2(x) \dot{x} + V'_{\text{ren}}(x) = G'(x) F, \quad (36)$$

and F becomes a white Gaussian noise.

Comparison between Eqs. (14) and (36) reveals that, for both cases of discrete and continuous spectrum baths, the linear coupling is the source of the induced linear damping and the shift in the eigenfrequency of the resonator, and the nonlinear coupling leads to nonlinear damping and modifications in the nonlinear conservative terms of the resonator. However, for the case of a continuous spectrum bath there are also fluctuating back-action terms that come along with the damping terms and balance them, i.e., the linear damping is associated with an additive noise term $2\langle g \rangle G'^2(0) \dot{x} \longleftrightarrow G'(0) \tilde{F}$ and the nonlinear damping with a multiplicative noise $2\langle g \rangle [G'^2(x) - G'^2(0)] \dot{x} \longleftrightarrow [G'(x) - G'(0)] \tilde{F}$.

References

1. Torteman, B., Kessler, Y., Liberzon, A., Krylov, S.: Microbeam resonator parametrically excited by electro-thermal Joule's heating and its use as a flow sensor. *Nonlinear Dyn.* **1**–15 (2019). <https://doi.org/10.1007/s11071-019-05031-4>
2. Krakover, N., Maimon, R., Tepper-Faran, T., Gerson, Y., Rand, R., Krylov, S.: Mechanical superheterodyne and its use for low frequency vibrations sensing. *J. Microelectromech. Syst.* **28**(3), 362 (2019)
3. Pelliccia, L., Cacciamani, F., Farinelli, P., Sorrentino, R.: High- Q tunable waveguide filters using ohmic RF MEMS switches. *IEEE Trans. Microw. Theory Tech.* **63**(10), 3381 (2015)
4. Kostsov, E., Sokolov, A.: Gigahertz MEMS clock generator. *Optoelectron. Instrum. Data Process.* **55**(2), 154 (2019)
5. Rebeiz, G.M., Muldavin, J.B.: RF MEMS switches and switch circuits. *IEEE Microw. Mag.* **2**(4), 59 (2001)
6. Rebeiz, G.M.: RF MEMS: theory, design, and technology. Wiley, New York (2004)
7. Nguyen, C.T.C.: MEMS technology for timing and frequency control. In: Proceedings of the 2005 IEEE International Frequency Control Symposium and Exposition, 2005.(IEEE, 2005), p. 11
8. Van Beek, J., Puers, R.: A review of MEMS oscillators for frequency reference and timing applications. *J. Micromech. Microeng.* **22**(1), 013001 (2011)
9. Rhoads, J.F., Shaw, S.W., Turner, K.L.: Nonlinear dynamics and its applications in micro-and nanoresonators. *J. Dyn. Syst. Meas. Control* **132**(3), 034001 (2010)
10. Cho, H., Jeong, B., Yu, M.F., Vakakis, A.F., McFarland, D.M., Bergman, L.A.: Nonlinear hardening and softening resonances in micromechanical cantilever-nanotube systems originated from nanoscale geometric nonlinearities. *Int. J. Solids Struct.* **49**(15–16), 2059 (2012)
11. Ruzziconi, L., Younis, M.I., Lenci, S.: An efficient reduced-order model to investigate the behavior of an imperfect microbeam under axial load and electric excitation. *J. Comput. Nonlinear Dyn.* **8**(1), 011014 (2013)

12. Zeng, J., Garg, A., Kovacs, A., Bajaj, A.K., Peroulis, D.: An equation-based nonlinear model for non-flat MEMS fixed-fixed beams with non-vertical anchoring supports. *J. Micromech. Microeng.* **25**(5), 055018 (2015)
13. Abdel-Rahman, E.M., Younis, M.I., Nayfeh, A.H.: Characterization of the mechanical behavior of an electrically actuated microbeam. *J. Micromech. Microeng.* **12**(6), 759 (2002)
14. Younis, M.I., Nayfeh, A.: A study of the nonlinear response of a resonant microbeam to an electric actuation. *Nonlinear Dyn.* **31**(1), 91 (2003)
15. Lifshitz, R., Cross, M.: Nonlinear dynamics of nanomechanical and micromechanical resonators. *Rev. Nonlinear Dyn. Complex.* **1**, 1 (2008)
16. Dykman, M., Krivoglaz, M.: Spectral distribution of nonlinear oscillators with nonlinear friction due to a medium. *Phys. Status Solidi (b)* **68**(1), 111 (1975)
17. Zaitsev, S., Shtempluck, O., Buks, E., Gottlieb, O.: Nonlinear damping in a micromechanical oscillator. *Nonlinear Dyn.* **67**(1), 859 (2012)
18. Amabili, M.: Derivation of nonlinear damping from viscoelasticity in case of nonlinear vibrations. *Nonlinear Dyn.* **93**(1), 5–18 (2018)
19. Dykman, M., Krivoglaz, M.: Theory of nonlinear oscillator interacting with a medium. *Sov. Phys. Rev.* **5**, 265 (1984)
20. Levantino, S., Samori, C., Zanchi, A., Lacaita, A.L.: AM-to-PM conversion in varactor-tuned oscillators. *IEEE Trans. Circuits Syst. II: Analog Digit. Signal Process.* **49**(7), 509 (2002)
21. Eichler, A., Moser, J., Chaste, J., Zdrojek, M., Wilson-Rae, I., Bachtold, A.: Nonlinear damping in mechanical resonators made from carbon nanotubes and graphene. *Nat. Nanotechnol.* **6**(6), 339 (2011)
22. DeMartini, B.E., Rhoads, J.F., Turner, K.L., Shaw, S.W., Moehlis, J.: Linear and nonlinear tuning of parametrically excited MEMS oscillators. *J. Microelectromech. Syst.* **16**(2), 310 (2007)
23. Saghafi, M., Dankowicz, H., Lacarbonara, W.: Nonlinear tuning of microresonators for dynamic range enhancement. *Proc. R. Soc. A* **471**(2179), 20140969 (2015)
24. Li, L.L., Polunin, P.M., Dou, S., Shoshani, O., Scott Strachan, B., Jensen, J.S., Shaw, S.W., Turner, K.L.: Tailoring the nonlinear response of MEMS resonators using shape optimization. *Appl. Phys. Lett.* **110**(8), 081902 (2017)
25. Antonio, D., Zanette, D.H., López, D.: Frequency stabilization in nonlinear micromechanical oscillators. *Nat. Commun.* **3**, 806 (2012)
26. Güttinger, J., Noury, A., Weber, P., Eriksson, A.M., Lagoin, C., Moser, J., Eichler, C., Wallraff, A., Isacsson, A., Bachtold, A.: Energy-dependent path of dissipation in nanomechanical resonators. *Nat. Nanotechnol.* **12**(7), 631 (2017)
27. Chen, C., Zanette, D.H., Czaplewski, D.A., Shaw, S., López, D.: Direct observation of coherent energy transfer in nonlinear micromechanical oscillators. *Nat. Commun.* **8**, 15523 (2017)
28. Shoshani, O., Shaw, S.W., Dykman, M.I.: Anomalous decay of nanomechanical modes going through nonlinear resonance. *Sci. Rep.* **7**(1), 18091 (2017)
29. Einstein, A., Hopf, L.: Statistical investigation of a resonator's motion in a radiation field. *Ann. Phys.* **33**, 1105 (1910)
30. Bogolyubov, N.: On some statistical methods in mathematical physics. *Izdat. Akad. Nauk Ukr. SSR Kiev* **1**, 115–137 (1945)
31. Atalaya, J., Kenny, T.W., Roukes, M., Dykman, M.: Nonlinear damping and dephasing in nanomechanical systems. *Phys. Rev. B* **94**(19), 195440 (2016)
32. Caldeira, A.O., Leggett, A.J.: Path integral approach to quantum Brownian motion. *Phys. A: Stat. Mech. Its Appl.* **121**(3), 587 (1983)
33. Matheny, M., Villanueva, L., Karabalin, R., Sader, J.E., Roukes, M.: Nonlinear mode-coupling in nanomechanical systems. *Nano Lett.* **13**(4), 1622 (2013)
34. Zhang, M., Wiederhecker, G.S., Manipatruni, S., Barnard, A., McEuen, P., Lipson, M.: Synchronization of micromechanical oscillators using light. *Phys. Rev. Lett.* **109**(23), 233906 (2012)
35. Nayfeh, A.H., Mook, D.T.: *Nonlinear Oscillations*. Wiley, New York (2008)
36. Guckenheimer, J., Holmes, P.J.: *Nonlinear Oscillations, Dynamical Systems, and Bifurcations of Vector Fields*, vol. 42. Springer, Berlin (2013)
37. Dirac, P.A.M.: *The Principles of Quantum Mechanics*, vol. 27. Oxford University Press, Oxford (1981)
38. Novotny, L.: Strong coupling, energy splitting, and level crossings: a classical perspective. *Am. J. Phys.* **78**(11), 1199 (2010)
39. Pardo, M., Sorenson, L., Ayazi, F.: An empirical phase-noise model for MEMS oscillators operating in nonlinear regime. *IEEE Trans. Circuits Syst. I: Regul. Pap.* **59**(5), 979 (2012)
40. Agrawal, D.K., Seshia, A.A.: An analytical formulation for phase noise in MEMS oscillators. *IEEE Trans. Ultrason. Ferroelectr. Freq. Control* **61**(12), 1938 (2014)
41. Pankratz, E., Sánchez-Sinencio, E.: Survey of integrated-circuit-oscillator phase-noise analysis. *Int. J. Circuit Theory and Appl.* **42**(9), 871 (2014)
42. Sobreviela, G., Vidal-Álvarez, G., Riverola, M., Uranga, A., Torres, F., Barniol, N.: Suppression of the Af-mediated noise at the top bifurcation point in a MEMS resonator with both hardening and softening hysteretic cycles. *Sens. Actuators A: Phys.* **256**, 59 (2017)
43. Dykman, M., Krivoglaz, M.: Classical theory of nonlinear oscillators interacting with a medium. *Phys. Status Solidi (b)* **48**(2), 497 (1971)
44. Habib, S., Kandrup, H.E.: Nonlinear noise in cosmology. *Phys. Rev. D* **46**(12), 5303 (1992)
45. Millonas, M.M.: Self-consistent microscopic theory of fluctuation-induced transport. *Phys. Rev. Lett.* **74**(1), 10 (1995)
46. Hänggi, P.: Generalized Langevin equations: a useful tool for the perplexed modeller of nonequilibrium fluctuations? In: Schimansky-Geier, L., Pöschel, T. (eds.) *Stochastic Dynamics*, pp. 15–22. Springer, Berlin (1997)